GEOMETRY MODIFICATIONS OF NONPLANAR WING TIP DESIGN FOR ADAPTATION TO LOW SPEED RANGE

A. Büscher, Th. Streit, C.-H. Rohardt
*Braunschweig Technical University, Institute of Fluid Mechanics,
Bienroder Weg 3, 38106 Braunschweig, Germany,
**German Aerospace Center (DLR), Institute of Aerodynamics and Flow Technology,
Lilienthalplatz 7, 38108 Braunschweig, Germany

Keywords: *wing tip device, winglet, nonplanar, low speed, M-DAW*

Abstract

An assessment study of wing tip devices at low speed is described. Designed at cruise, the device provides poor low speed performance due to large regions of flow separation. Both airfoil redesign and the usage of moving parts on the leading edge are investigated to gain the flow behaviour. This study was done in two stages using a clean configuration at low speed and furthermore a take-off geometry at high-lift. Both techniques provide beneficial impact on the aerodynamic behaviour at low speed regime.

1   Nomenclature

c	:	chord length
c_D	:	drag coefficient
Δc_D	:	difference in c_D between investigated and reference configuration
c_{fx}	:	friction coefficient component in freestream direction
c_L	:	lift coefficient
c_p	:	pressure coefficient
M	:	Mach number
Re	:	Reynolds number
x, y, z	:	Cartesian coordinates
η	:	dimensionless span
Suffices		
equiv	:	equivalent drag component
*	:	critical value

2   Introduction

Winglets have been used for a long time to improve the performance of aircraft by reducing the drag due to lift. Unfortunately, the designs promising adequate aerodynamic benefit cause an increase in load and wing root bending moment. The resulting strengthening of the structure leads to an increase in weight, which reduces or even balances the aerodynamic gain found. To consider the relationship between aerodynamic and structural impact, a corresponding objective function was provided for design at cruise. This paper addresses the low speed behaviour of the novel device designed. For improving this speed regime, the potential of redesigned winglet airfoils and the usage of movable leading edge devices are investigated and assessed using CFD. After studying a clean configuration at low speed, a further geometry with a high-lift system is tested. All beneficial effects are given relative to a planar reference configuration.

3   Methodology

3.1   Numerical method

For design and assessment work the RANS-code TAU was used. The TAU code [1] solves the compressible three-dimensional Reynolds-averaged Navier-Stokes equations on hybrid grids. It was developed by DLR Göttingen and DLR Braunschweig. Hexahedral, prismatic,

pyramedal, and tetrahedral types of cells are supported. For turbulence modelling, both the Spalart-Allmaras model with Edwards modification (SAE) [2] and the Menter shear-stress transport-model (MSST) [3] were used. The CPU runtime was reduced by a multigrid technique and parallel computations.

3.2   Geometries

The geometry provided within the design study is a long-range research configuration of Airbus UK. The model is a wing-body configuration. It provides a wing planform with $35.9°$ swept leading edge, a dihedral of $7.6°$, and a taper ratio of 0.211. The basic geometry has an aspect ratio of 8.0 and a semispan of $39.5\,m$. The fuselage measures a length of $70.4\,m$.

The model may be equipped either with a planar Küchemann wing tip or a nonplanar wing tip device. The latter is a conventional large winglet with a dihedral of $49.3°$ and a leading edge sweep of $38.3°$. Its length of $5.3\,m$ increases the semispan of the configuration by $3\,m$. The model was used at high-speed and low-speed regime. The planform of the reference configuration is shown in Fig. 1.
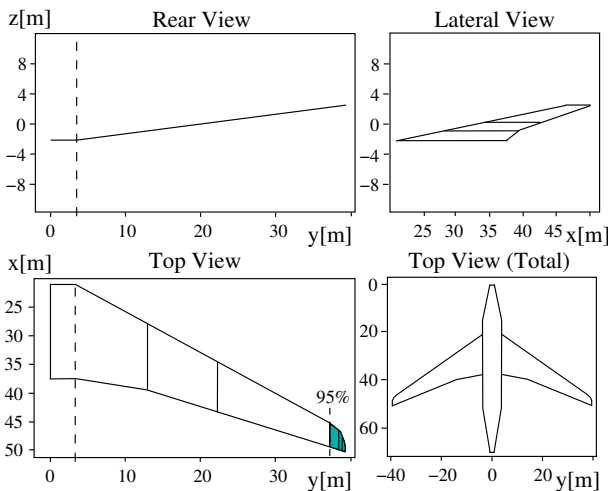
Fig. 1 Schematic of wing planform with reference wing tip

A slightly different configuration with take-off settings was studied for high lift. While the former model is a wing-body geometry only, the latter also contains nacelles. Except the most outer 5% of semispan, slats are deployed along the wing for take-off. Flaps and ailerons are deflected. The flaps are in extended position. The fuselages of both models differ slightly in length.

4   Results and discussion

4.1   Preceding studies at cruise

Previous investigations are summarised briefly in this paper to provide all the information needed. Büscher et al. [4] describe the preceding studies in detail.

For the design work at high speed, an objective function was given in form of an equivalent drag reduction $\Delta c_{D_{equiv}}$ relative to the reference wing with planar wing tip. The main terms account for drag increments due to the aerodynamic drag reduction and due to weight increase via wing root bending moment (*WRBM*) increase and device weight. Note, the impact of the increase in bending moment on the equivalent drag was weighted strongly. The objective function was prepared by Airbus UK.

Based on the design approach, several parametric studies were carried out at high speed design point modifying sweep, dihedral, span, chord length, taper, and twist of various wing tip devices. The maximum semispan is limited to $42.5\,m$, which corresponds to a semispan increase of $3\,m$ compared to the reference wing. The wing tip device can change the wing geometry only outboard of 95% of the wing semispan. The ground handling requirements of the aircraft are considered by a limited vertical extension of the wing tip device.

The optimum found is a highly swept anhedral wing tip device with small chord length, shown in Fig. 2. A potential negative impact of anhedral wing tip devices on the aerodynamic performance [5] is outbalanced by the beneficial effect on the *WRBM*. The gain found is caused by the negative dihedral of the wing. Additional benefit in wing root bending moment was obtained by off-loading the region of the wing-
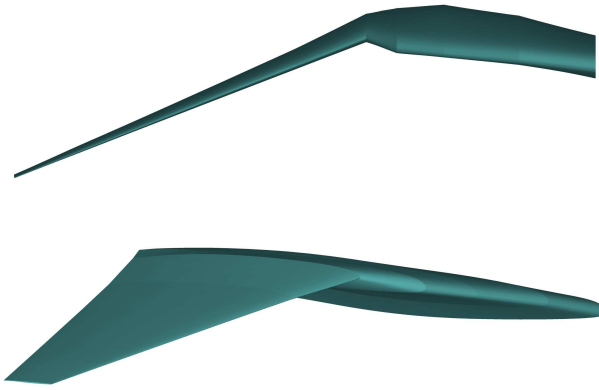
Fig. 2 Visualisation Of The Anhedral Winglet From Front View (**Top**) And Lateral View (**Bottom**)

Fig. 4 Equivalent Drag Reduction Relative To Küchemann, TAU result, $M = 0.85$, $Re = 54.2 \cdot 10^6$

winglet junction. Both modifications are based on the strong significance of the *WRBM* within the design approach. Correspondingly, the aerodynamic drag reduction is smaller compared to the large winglet (see Fig. 3).

Fig. 3 Drag Reduction Relative To Küchemann, TAU result, $M = 0.85$, $Re = 54.2 \cdot 10^6$

However, the novel design shows a gain in $\Delta c_{D_{equiv}}$ relative to the reference Küchemann wing tip as well as to the large winglet at design point. Fig. 4 shows that even at off-design the performance improvement depending on aerodynamic drag, wing root bending moment, and device weight is clearly visible. Since the lift has an quadratic dependency on induced drag, the large winglet equalises the drag gain at very high incidence.

4.2 Validation of numerical methods

For validation of the clean configuration at low speed, ETW [6] wind tunnel results of both reference configurations are available. All RANS solutions have been performed using TAU (see section 3.1). Validation data obtained previously using TAU at low speed may be given in [7]. The grid generation needed for RANS solutions employs 36 prisms in normal direction around the surfaces in order to resolve the boundary layer. The first cell spacing was set satisfactorily with respect to the existing Reynolds number of $7.2 \cdot 10^6$. Two adaptations were conducted to refine the regions of strong gradients as leading edge and area of flow separation. The corresponding grids result in total point numbers of 11.7 million and 15.5 million respectively. Note that the grid parts, including the geometry of fuselage and wing up to a spanwise position of $\eta = 0.95$, are identical in cases with different wing tip devices. In addition to the low speed design point, two further incidences were investigated. In this study, only the Spalart-Allmaras turbulence model with Edwards modification [2] was used.

Fig. 5 shows the pressure distribution of both configurations at an inboard position. TAU agrees very well with the experimental data.

The rigid CAD geometry used for computations was generated to match the shape of the wind tunnel model at cruise design point. Due
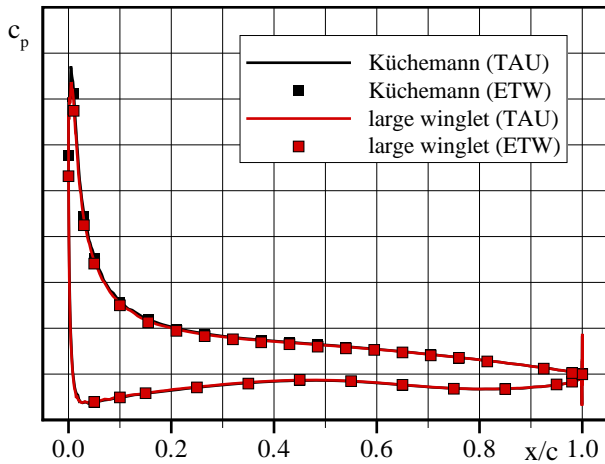
Fig. 5 Pressure Distributions On Spanwise Station $\eta = 0.47$, $c_L = 1.0$, $M = 0.2$, $Re = 7.2 \cdot 10^6$

to differing wing twist and bending of the model during the low speed test, small differences between numerical and experimental geometries may cause discrepancies in the outboard regions of the wing [8]. Fig. 6 shows small discrepancies in the suction peak region. Note, the differences seem to be larger for the planar geometry.
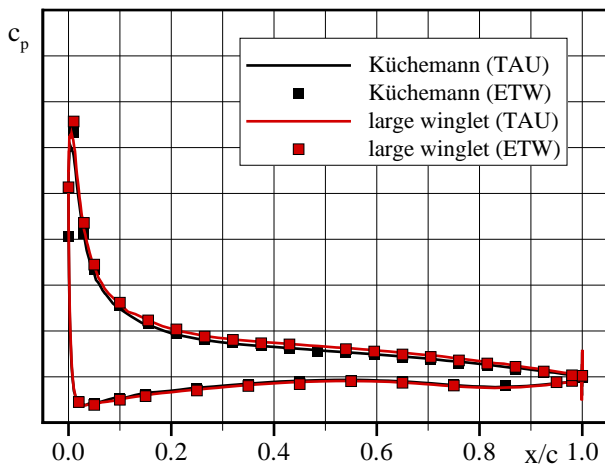
Fig. 6 Pressure Distributions On Spanwise Station $\eta = 0.95$, $c_L = 1.0$, $M = 0.2$, $Re = 7.2 \cdot 10^6$

Fig. 7 provides two additional cut sections at $\eta = 0.99$ and $\eta = 1.04$ for the conventional winglet. Note the former station is still placed on the planar part, while the latter one is positioned at half winglet length. The results agree

well. Due to the lack of pressure tappings close to the leading edge, expected discrepancies in this region cannot be shown.
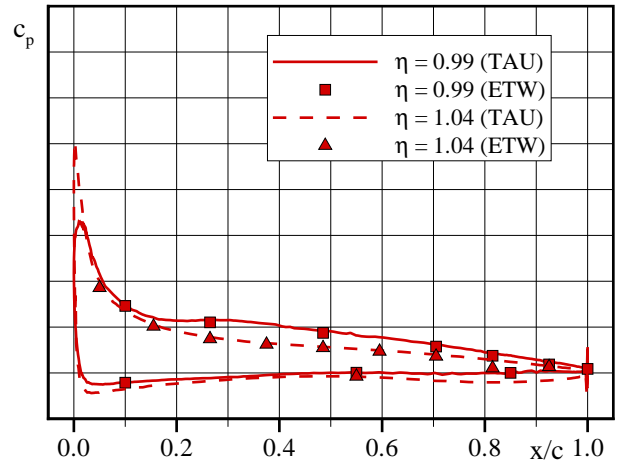
Fig. 7 Pressure Distribution Of Large Winglet, $c_L = 1.0$, $M = 0.2$, $Re = 7.2 \cdot 10^6$

Fig. 8 shows the drag reduction of the large winglet in comparison to the planar reference geometry. The TAU results provide a constant offset of around 1% compared to the wind tunnel curve. Some of these discrepancies may also be explained by deformation of the wind tunnel model. However, the drag increments are in good agreement to each other.
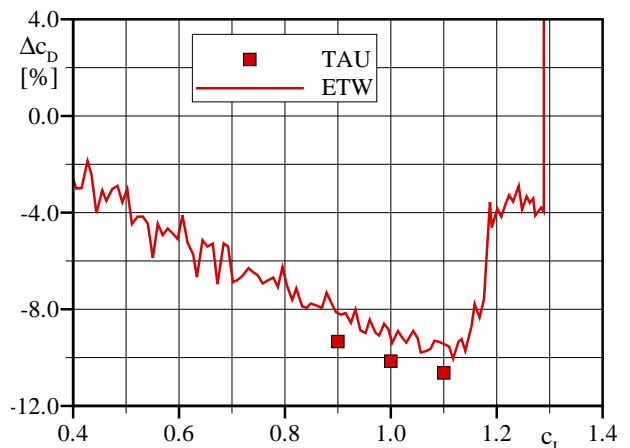
Fig. 8 Drag Reduction Of Large Winglet Relative To Küchemann, $M = 0.2$, $Re = 7.2 \cdot 10^6$

4

4.3 Aerodynamic performance at low speed conditions

No additional design study was carried out at low speed. Unlike the cruise case, the impact of *WRBM* and device weight are of no interest at low speed. For the latter, only the aerodynamic performance is relevant to reduce emission and noise.

Based on the good agreement presented in the previous section, TAU was used to investigate the low speed performance of the anhedral design. Note, only the grid outside of $\eta = 0.95$ is modified in comparison to the mesh of the reference geometry. The grid has a total point number of 15.7 million.

Computations using the novel device were performed at the same fixed lift coefficients as the reference configurations. Fig. 9 shows the drag benefit of the anhedral winglet. Since the large winglet exceeds the anhedral winglet in length, a greater drag gain by the conventional wing tip device was assumed due to lower induced drag.
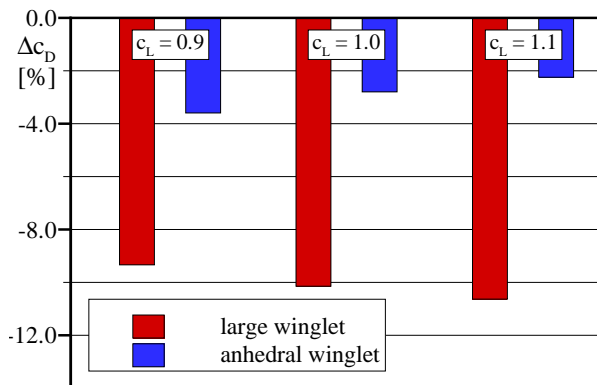
Fig. 9 Drag Reduction Of Different Wing Tip Devices Relative To Küchemann, TAU results, $M = 0.2$, $Re = 7.2 \cdot 10^6$

However, the lost of drag benefit with increasing angle of attack relative to the Küchemann indicates an increase of viscous drag, which has to be caused by significant flow separation. Note, the remaining drag benefit in comparison to the reference wing tip results from the induced drag gain due to the increased span.

This assumption is confirmed by Fig. 10.

Large regions of the anhedral device contain reversed flow at $c_L = 0.9$. This trend continues increasing the angle of attack.
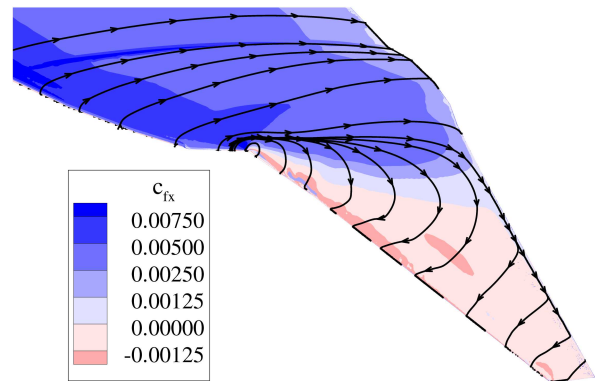
Fig. 10 Streamtraces and c_{fx} contour plot for anhedral winglet, $c_L = 0.9$, $M = 0.2$, $Re = 7.2 \cdot 10^6$

Fig. 11 shows that the nonplanar part of the novel tip device is separated entirely. The poor flow behaviour at low speed is mainly caused by the impact of the *WRBM* within the design objective at cruise and the corresponding load distribution. Furthermore, high local lift coefficients exist in the region of the device due to its very small chord length.
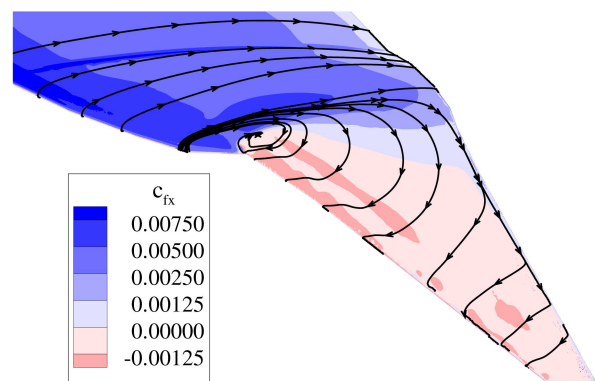
Fig. 11 Streamtraces and c_{fx} contour plot for anhedral winglet, $c_L = 1.0$, $M = 0.2$, $Re = 7.2 \cdot 10^6$

For improving the low speed performance without deteriorating the cruise condition, two options are presented in the following sections.

4.4   Redesign of winglet airfoil

An option to improve the low speed behaviour of the novel device is a redesign of the employed winglet airfoils. This approach requests an assessment at high speed subsequently to prove that no penalty at cruise condition appears. This procedure might be conducted iteratively.

4.4.1   Design work and assessment at cruise

There was no large potential to improve the low speed characteristics by changing the nose radius due to the small airfoil thickness . Instead, an airfoil with a completely different pressure characteristic for the upper surface was designed. During design, the original and the redesigned airfoils were analysed using 3D-RANS solutions for the wing-body configuration with large winglet mounted. To account for the large local lift of the anhedral winglet due to the reduced chord length, the local twist of the basic large winglet was modified by an increase of $1°$ in the region $\eta > 1.0$. To ensure the same load and induced drag in case of using the new airfoil, the twist outboard of $\eta > 0.95$ was obtained by matching the load distribution of the modified large winglet case with basic airfoil.
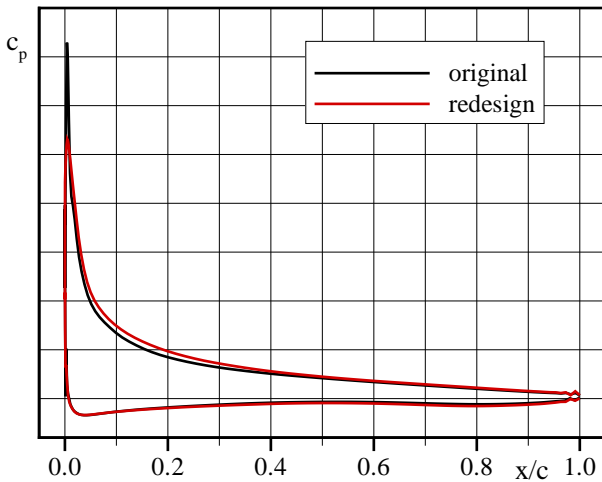
Fig. 12 Pressure distributions of large winglet using original and redesigned airfoils, $\eta = 1.04$, $\alpha = 12.5°$, $M = 0.2$, $Re = 7.2 \cdot 10^6$

The design process of the new winglet airfoil was done in several steps iteratively by high speed assessment of those geometries, that were found at low speed. In Fig. 12, low speed pressure distributions are compared for the modified basic and the final redesigned airfoil. The new airfoil reduces the nose suction peak. The corresponding global coefficient indicates that at moderate incidence, the aerodynamic drag is reduced significantly and the lift is increased slightly.
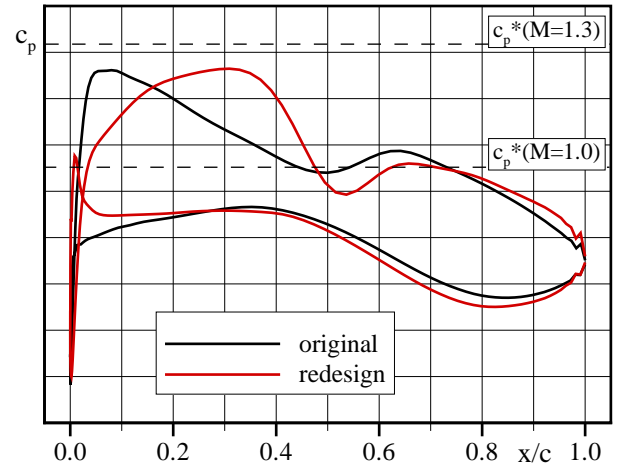
Fig. 13 Pressure distributions of large winglet using original and redesigned airfoils, $\eta = 1.04$, $c_L = 0.5$, $M = 0.85$, $Re = 54.2 \cdot 10^6$

Fig. 13 shows mid-winglet pressure distributions of both cases at cruise design point. The suction peak is shifted backward and no stronger shock is clearly discernible. Thus, the resulting drag coefficient of the geometry with redesign airfoils is only increased weakly in comparison to the basic configuration.

4.4.2   Application to anhedral winglet

Based on the previous results, the original and the redesigned airfoil were analysed using 3D-RANS solutions for the wing-body configuration including the anhedral winglet. As described above, the twist of the new airfoil case for $\eta > 0.95$ was obtained by matching the load distribution of the anhedral winglet with original airfoil at cruise speed.

Drag increments relative to the Küchemann configuration are shown in Fig. 14. At $c_L = 0.9$ the drag reduction in comparison to the Küchemann tip is gained by more than 2%. Unfortu-

nately, this beneficial effect may be conserved only partially with increasing incidence. Thus, the drag improvement is almost gone at $c_L = 1.1$.
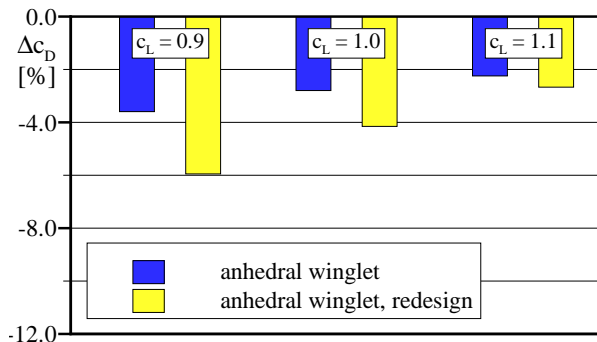
Fig. 14 Drag Reduction Of Different Wing Tip Devices Relative To Küchemann, TAU results, $M = 0.2$, $Re = 7.2 \cdot 10^6$

A corresponding result is visible in Fig. 15 and Fig. 16. Comparing the former one with Fig.10, a big improvement is visible due to the limitation of the region containing reversed flow to the outer 30% of the tip device.
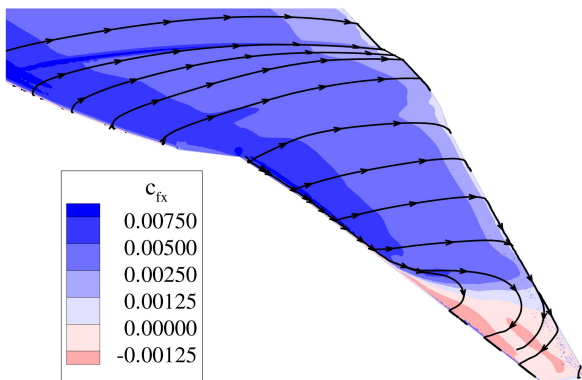
Fig. 15 Streamtraces and c_{fx} contour plot for anhedral winglet with redesigned airfoils, $c_L = 0.9$, $M = 0.2$, $Re = 7.2 \cdot 10^6$

Fig. 16 shows the c_{fx} plot at increased lift coeffcient. The nonplanar part of the anhedral winglet is almost separated completely and shows only small advantage compared to the device with original airfoil (see Fig. 11).

A c_p comparison relative to the anhedral configuration using the original airfoil was performed in an outboard spanwise section at cruise
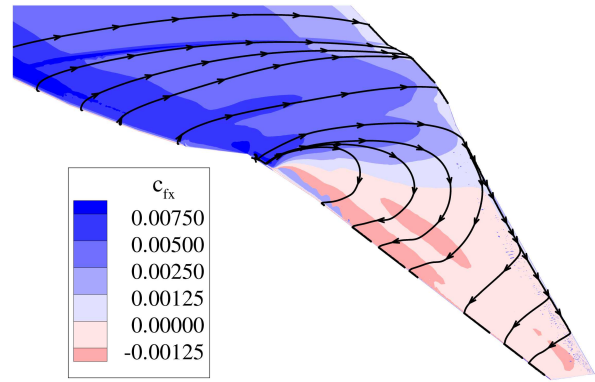
Fig. 16 Streamtraces and c_{fx} contour plot for anhedral winglet with redesigned airfoils, $c_L = 1.0$, $M = 0.2$, $Re = 7.2 \cdot 10^6$

design point (not shown here). Note that despite of the greater local lift of the anhedral winglets, no shocks appear. Since there is no indication of wave drag increase in the winglet region, $\Delta c_{D_{equiv}}$ does not increase at cruise.

4.5 Moving part on leading edge

The general potential of leading edge devices to improve low speed performance was already shown successfully [9].

The final geometry of the movable device was obtained by varying the relative device length and the deflection angle using viscous-coupled 2D-Euler solver. The leading edge device with a relative length of 20% is downward deflected by $20°$. Unlike a trailing edge device, the deflection of the leading edge device increases the local maximum lift coefficient without changing the spanwise load. This way, the induced drag is very similar to the nondeflected anhedral winglet. The viscous drag is reduced. Since the moving parts consist of hinged devices without gaps, the parasitic drag is of very low level.

The resulting overall drag gain compared to the Küchemann wing tip is visible in Fig. 17. The leading edge device provides a drag gain of about 4% compared to the basic anhedral geometry. The improvement relative to the reference configuration is even greater than 6.5%. Note, that unlike the previous case using redesigned air-

foils, this benefit may be kept for higher lift coefficients as well.
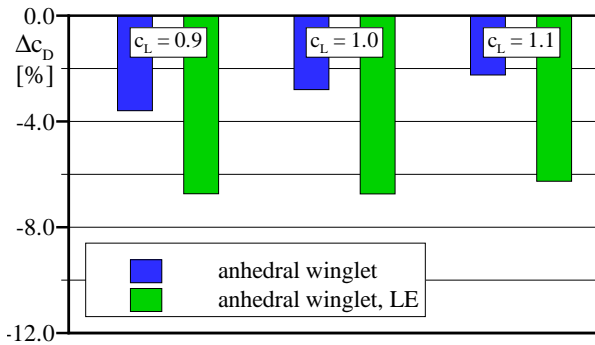
Fig. 17 Drag Reduction Of Different Wing Tip Devices Relative To Küchemann, TAU results, $M = 0.2$, $Re = 7.2 \cdot 10^6$

The large improvement may be seen in the c_{fx} plot at $c_L = 0.9$ (see Fig. 18). No flow separation exists any more, except in the most outer part of the winglet as well as in the inner region of the movable device.
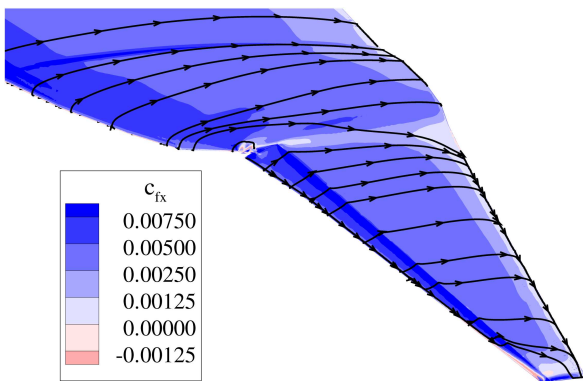
Fig. 18 Streamtraces and c_{fx} contour plot for anhedral winglet with leading edge device, $c_L = 0.9$, $M = 0.2$, $Re = 7.2 \cdot 10^6$

Increasing the incidence, Fig. 19 shows the corresponding c_{fx} pattern. The region containing flow separation is enlarged slightly from outboard to inboard. Note, the flow field promises better performance than the one provided by the anhedral winglet with redesigned airfoil at lower lift coefficient.
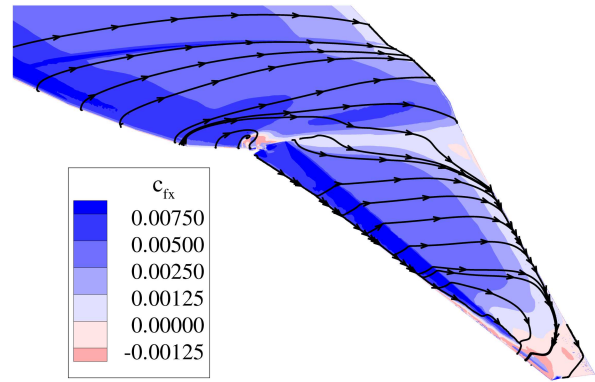
Fig. 19 Streamtraces and c_{fx} contour plot for anhedral winglet with leading edge device, $c_L = 1.0$, $M = 0.2$, $Re = 7.2 \cdot 10^6$

4.6 Investigation on take-off configuration

Based on the promising results using the clean configuration at low speed, a further study at high lift was carried out. For take-off condition, another model geometry was investigated (see section 3.2). A validation study on this geometry using both the Küchemann tip and the conventional large winglet was already conducted successfully [9]. The same grids were used in the present study. For the different configurations of the anhedral winglet, only the outer 5% of the wing were remeshed to allow the best comparison. In addition to the results using the SAE turbulence model [2], some computations based on the Menter SST model [3] were made. The previous contour plots of the anhedral winglet at low speed have shown strong flow separation, which may be predicted better by the 2-equation turbulence model.

Fig. 20 shows the drag reduction of all investigated wing tip devices relative to the Küchemann. For comparison experimental data from a KKK wind tunnel measurement [10] were added. The results of both turbulence models provide similar accuracy.
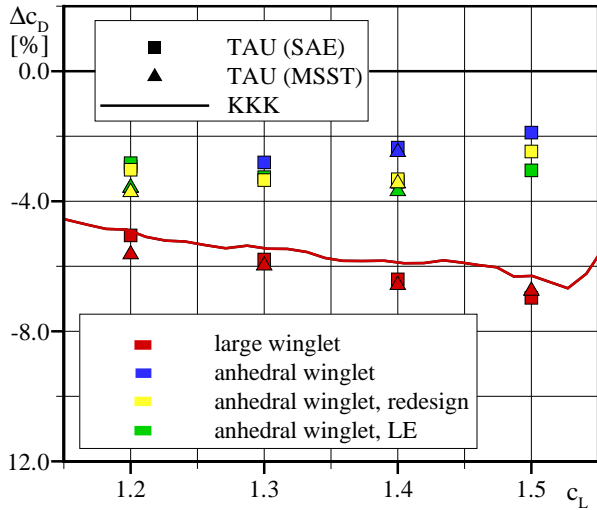
Fig. 20 Drag Reduction Of Different Wing Tip Devices Relative To Küchemann, $M = 0.2$, $Re = 7.2 \cdot 10^6$

Fig. 21 shows separated flow for large regions of the anhedral winglet. Note, the extension of these regions is similar to the contour pattern provided by the clean configuration at $c_L = 1.0$.
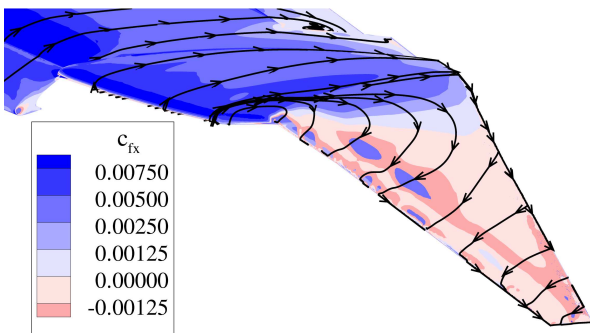
Fig. 21 Streamtraces and c_{fx} contour plot for anhedral winglet, MSST, $c_L = 1.4$, $M = 0.2$, $Re = 7.2 \cdot 10^6$

The case of the new winglet airfoil provides a good performance benefit (see Fig. 22). Almost half of the planar part of the winglet contains attached flow. This improvement compared to the nonmodified geometry is bigger than the gain shown for wing-body configuration at low speed.
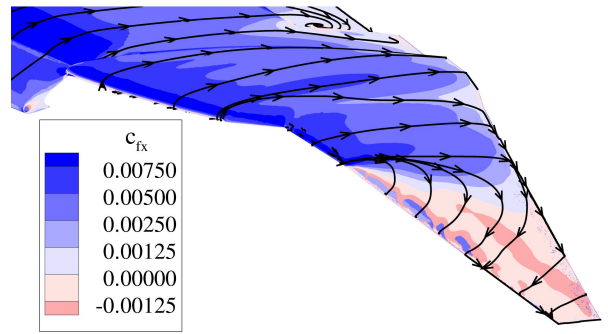
Fig. 22 Streamtraces and c_{fx} contour plot for anhedral winglet with redesigned airfoils, MSST, $c_L = 1.4$, $M = 0.2$, $Re = 7.2 \cdot 10^6$

The corresponding c_{fx} pattern using the leading edge device is visualised in Fig. 23. A spatial limitation of the flow separation due to the device deflection is clearly visible. However, the improvement is of lower level compared to previous results using the clean configuration. Furthermore, the advantage to the model with redesigned airfoil is clearly smaller.
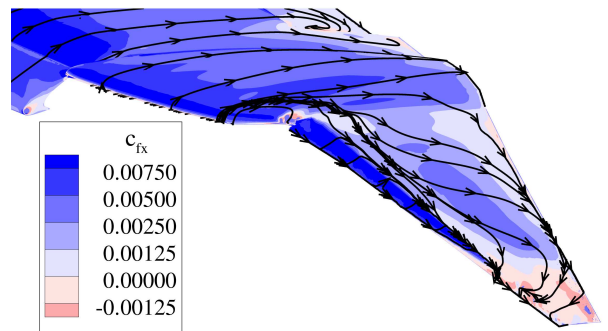
Fig. 23 Streamtraces and c_{fx} contour plot for anhedral winglet with leading edge device, MSST, $c_L = 1.4$, $M = 0.2$, $Re = 7.2 \cdot 10^6$

5   Conclusions

A novel wing tip device, which was designed at cruise speed, has been assessed at low speed condition. The RANS-code TAU was used for the assessment study. For the reference configuration and a conventional winglet, the TAU solutions agree very well with the experimental data. The low-speed performance of the novel wing tip device is relatively poor due to the design con-

straints at cruise. Large regions of flow separation occured. Therefore, the usage of redesigned winglet airfoils and a leading edge device were analysed. Both approaches increased the present drag benefit relative to the reference wing. Additionally, the same comparison was made using the corresponding take-off configuration. The trends found for the clean geometry could be confirmed but are of lower level. Particularly, the leading edge device showed different benefit in the flow behaviour comparing both configurations. Concluding, both geometry modifications improve the low speed performance of the novel wing tip device without causing penalty at high speeds.

6   Acknowledgement

References

[1] Gerhold, T. *Overview of the hybrid RANS code TAU.*
MEGAFLOW - Numerical flow simulation for aircraft design, edited by N. Kroll and J. Fassbender,
Notes on numerical fluid mechanics and multidisciplinary design, Vol. 89, Springer, Berlin, Heidelberg, 2005, pp. 81-92

[2] Edwards, J. R.; and Chandra, S. *Comparison of eddy viscosity-transport turbulence models for three-dimensional, shock-separated flowfields.*
AIAA Journal, Vol. 34, No. 4, pp. 756-763, 1996

[3] Menter, F. R. *Two-equation eddy-viscosity turbulence models for engineering applications.*
AIAA Journal, Vol. 32, No. 8, pp. 1598-1605, 1994

[4] Büscher, A.; Radespiel, R.; and Streit, Th. *Modelling and design of wing tip devices at various flight conditions using a databased aerodynamic prediction tool.*
Aerospace Science and Technology, accepted for publication

[5] Leyser, J. *Accurate computation of lift and induced drag at lifting surfaces.*
AIAA Paper 96-2405-CP, 1996

[6] European Transonic Windtunnel (ETW).
http://www.etw.de

[7] Melber-Wilkending, S.; Rudnik, R.; Ronzheimer, A.; and Schwarz, T. *Verification of MEGAFLOW-software for high lift applications.*
MEGAFLOW - Numerical flow simulation for aircraft design, edited by N. Kroll and J. Fassbender,
Notes on numerical fluid mechanics and multidisciplinary design, Vol. 89, Springer, Berlin, Heidelberg, 2005, pp. 135-163

[8] Elsholz, E.; and Barakat, S.: *CFD analysis of twist correction on commercial aircraft wing with different tip devices in ETW windtunnel.*
AIAA Paper 2006-0513, 2006

[9] Büscher, A.; Mertol, B. A.; and Radespiel, R. *Improving high lift behaviour of nonplanar wing tip devices using moving parts.*
CEAS/KATnet Conference on Key Aerodynamic Technologies, Bremen, 20-22 June 2005

[10] Cryogenic wind tunnel Cologne (KKK).
http://www.dnw.aero/facilities/kkk

[11] Modelling and Design of Advanced Wing tip devices.
European Union Project No. G4RD-CT-2002-00837

[12] Norddeutscher Verbund für Hoch- und Höchstleistungsrechnen.
http://www.hlrn.de